

The possible coexistence of superconductivity and topological electronic states in 1T-RhSeTe

Tengdong Zhang¹, Rui Fan³, Yan Gao¹, Yanling Wu¹, Xiaodan Xu¹, Dao-Xin Yao^{2,*} and Jun Li^{1†}

¹Key Laboratory for Microstructural Material Physics of Hebei Province,
School of Science, Yanshan University, Qinhuangdao 066004, China.

²State Key Laboratory of Optoelectronic Materials and Technologies,
Guangdong Provincial Key Laboratory of Magnetoelectric Physics and Devices,
School of Physics, Sun Yat-Sen University, Guangzhou 510275, Peoples Republic of China.

³School of Physics, Beijing Institute of Technology, Beijing 100081, China

Transition metal dichalcogenides (TMDs), exhibit a range of crystal structures and topological quantum states. The 1T phase, in particular, shows promise for superconductivity driven by electron-phonon coupling, strain, pressure, and chemical doping. In this theoretical investigation, we explore 1T-RhSeTe as a novel type of TMD superconductor with topological electronic states. The optimal doping structure and atomic arrangement of 1T-RhSeTe are constructed. Phonon calculations validate the integrity of the constructed doping structure. The analysis of the electron-phonon coupling (EPC) using the Electron-phonon Wannier (EPW) method has confirmed the existence of a robust electron-phonon interaction in 1T-RhSeTe, resulting in total EPC constant $\lambda = 2.02$, the logarithmic average frequency $\omega_{\log} = 3.15$ meV and $T_c = 4.61$ K, consistent with experimental measurements and indicative of its classification as a BCS superconductor. The band structure analysis revealed the presence of Dirac-like band crossing points. The topological non-trivial electronic structures of the 1T-RhSeTe are confirmed via the evolution of Wannier charge centers (WCCs). Collectively, these distinctive properties underscore 1T-RhSeTe as a possible candidate for a topological superconductor, warranting further investigation into its potential implications and applications.

I. INTRODUCTION

Transition metal dichalcogenides (TMDs) are compounds represented by the chemical formula MX_2 , where M denotes transition metals such as Mo, W, and Ni, and X represents chalcogen elements such as S, Se, and Te. Featuring a layered structure, TMDs display a remarkable degree of diversity and exhibit a variety of topological quantum states, including Weyl semimetallic, topological insulator, and quantum spin Hall effect [1–4]. TMDs can adopt various crystal structures, with the most prevalent being hexagonal (2-H), rhombohedral (3-R), and trigonal (1-T) phases. The 2-H phase typically manifests as a semiconductor and is the most thermodynamically stable, while the 1-T phase exhibits metallic behavior and possesses distinctive topological properties [5–7].

The superconducting behaviors of 1-T phase TMDs are intrinsic or induced by chemical doping or applied strain [8–10]. For example, both 1T-TiSe₂ and 1T-PdTe₂ exhibit semimetallic characteristics, and the topological superconductivity can be driven by electron-phonon coupling. Experimental observations have revealed that 1T-TiSe₂ exhibits a critical temperature (T_c) of 2 K under a pressure of 3 GPa, while the T_c of PdTe₂ is 1.7 K [11, 12]. In the 1-T phases of PtTe₂, PdSe₂, NiTe₂, and PdTe₂, the Dirac cone is tilted, and forms a type-II Dirac topological point [13–16]. Furthermore, the Dirac point in NiTe₂ is situated at the Fermi energy level of 0.80 meV,

and the position of the Fermi energy can be adjusted through strain, pressure, and chemical doping [10]. 1T-phase TMDs hold significant promise for inducing superconductivity with topological quantum states.

In the broadest sense, a superconductor is regarded as topological if any of the topological numbers is nonzero [17, 18]. Topological superconductors have emerged as a fascinating area of research in quantum computing, due to their unique physical properties and potential applications [19–23]. They offer an ideal platform for studying fundamental quantum physics problems, such as non-abelian anyons and quantum entanglement, and propose possible solutions for building future quantum computers that can achieve fault-tolerant quantum computation [22–24]. Topological superconductors are closely associated with Majorana fermions, which are exotic particles that are their own antiparticles [23, 25].

A novel Dirac semimetal, 1T-RhSeTe, has been identified as a superconductor with $T_c = 4.72$ K [26]. In 1T-RhSeTe, selenium (Se) replaces tellurium (Te) atoms in the 1T phase of RhTe₂, a TMD previously reported to lack superconductivity and topological electronic states [27, 28]. This substitution induces superconductivity and topological electronic states, which is a possible candidate for topological superconductors.

This study employs density-functional theory (DFT) within first-principles calculations to examine the electronic bands, phonon, superconductivity, and topological characteristics of 1T-RhSeTe. Analysis of the electron-phonon coupling and Eliashberg spectral function yields the electron-phonon coupling strength ($\lambda = 2.02$) and $T_c = 4.61$ K.

Furthermore, a Dirac cone crosses near the Fermi en-

* yaodaax@mail.sysu.edu.cn

† ljcyj007@ysu.edu.cn

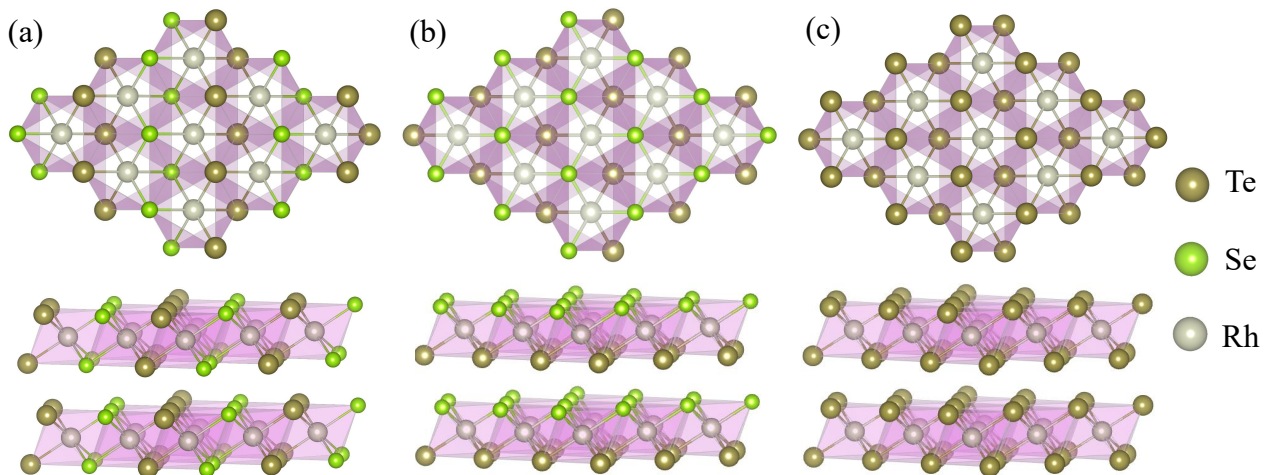


FIG. 1: Top and side views of the crystal structure of $1T$ -RhSeTe and RhTe₂: (a) type-I doping $1T$ -RhSeTe, where Se replaces Te atoms along lines; (b) type-II doping $1T$ -RhSeTe, where Se replaces Te atoms within plane; (c) $1T$ -RhTe₂.

TABLE I: Lattice constants for type-I, type-II $1T$ -RhSeTe, compare with experiment and $1T$ -RhTe₂

Structure	Lattices(Å)	Energy	Ref.
Type-I	a, b = 3.794, c = 5.363	-32.036 eV	calculate
Type-II	a, b = 3.818, c = 5.291	-32.012 eV	calculate
Exper.	a, b = 3.798, c = 5.389		Ref.[26]
RhTe ₂	a, b = 3.938, c = 5.513		Ref.[27]

ergy in the absence of SOC. However, the presence of the SOC effect result in the Dirac cone becoming gapped, thereby manifesting a Dirac-type surface state that is protected by time-reversal symmetry. The calculated \mathbb{Z}_2 topological index is $\mathbb{Z}_2 = 1$, indicating that $1T$ -RhSeTe is in a strongly topological electronic state.

II. COMPUTATIONAL DETAILS

We use the projector-augmented wave method implemented in the Vienna Ab initio Simulation Package (VASP) to perform density-functional theory (DFT) calculations for the structure optimization [29]. The generalized gradient approximation (GGA) and the Perdew Burke-Ernzerhof (PBE) function are used to treat the electron exchange-correlation potential[30, 31]. In the computation, the plane wave cut-off energy is set at 700 eV, a Monkhorst-Pack k lattice with a spacing of $2\pi \times 0.03 \text{ \AA}^{-1}$ is employed, and the structure is optimized using optB88-vdW van der Waals (vdW) interaction corrections [32] until the force on each atom less than $0.015 \text{ eV} \times \text{Å}^{-1}$.

Quantum Espresso (QE) is used for DFT calculations including self-consistent, band structure, and phonon calculations [33]. The PBE generalization of GGA is the ba-

sis for the exchange-correlation generalization. The calculations used kinetic energy cutoff values of 70 Ry for the wave function and 700 Ry for the potential function, a $6 \times 6 \times 6$ k-grid, and a $6 \times 6 \times 6$ q-point grid. The self-consistent convergence threshold is set to 1×10^{-10} Ry. The d-orbitals of the Rh atoms, the p-orbitals of the Te atoms, and the p-orbitals of the Se atoms are selected as the projected orbits, and the $6 \times 6 \times 6$ k-mesh grid is set up to construct the tight-binding Hamiltonian for the established structure by the software package wannier90 based on maximally localized wannier functions (MLWFs) [34, 35].

The Electron-phonon Wannier (EPW) code is employed to obtain the electron-phonon coupling and BCS superconductivity. The k-mesh and q-mesh grids are uniformly increased to $20 \times 20 \times 20$ for more accurate results. The EPW code solves the Eliashberg equation and related superconductivity equations to calculate electron-phonon coupling strength and T_c . The electron-phonon coupling constant λ , which can be calculated by

$$\lambda = 2 \int \frac{\alpha^2 F(\omega)}{\omega} d\omega, \quad (1)$$

where $\alpha^2 F(\Omega)$ is the Eliashberg spectral function, the phonon density of states weighted by an electron-phonon coupling matrix element at each k-point and frequency. The superconducting T_c is determined with the McMillan equation modified by Allen-Dynes formula [36, 37]

$$T_c = \frac{f_1 f_2 \omega_{log}}{1.2} \exp \left[\frac{-1.04(1 + \lambda)}{\lambda(1 - 0.62\mu^*) - \mu^*} \right], \quad (2)$$

where μ^* is the effective screened Coulomb repulsion constant typically ranging from 0.1 to 0.16 eV, and the logarithmically averaged frequency ω_{log} can be defined as

$$\omega_{log} = \exp \left[\frac{2}{\lambda} \int \frac{d\omega}{\omega} \alpha^2 F(\omega) \ln \omega \right]. \quad (3)$$

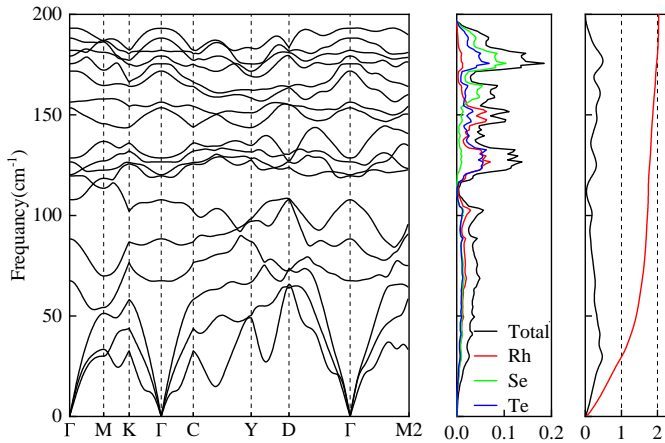


FIG. 2: The phonon spectrum of the 1T-RhSeTe, phonon density of states (PHDOS), and Eliashberg spectral function $\alpha^2 F(\omega)$.

We use WannierTools[38] to get WCCs [39] to reflect the topological properties of time-reversal invariant systems. \mathbb{Z}_2 topological invariant [40] is given by the number of times L any line crosses a WCCs line when going from $k_i = 0$ to $k_i = \pi$.

$$\mathbb{Z}_2 = L \pmod{2} \quad (4)$$

The topological properties of three-dimensional materials can be classified using the \mathbb{Z}_2 topological index, classified by a set of indices $(\nu; \nu_x \nu_y \nu_z)$ defined through the 2D invariants on the time-reversal invariant planes in the Brillouin zone

$$\nu = \mathbb{Z}_2(k_i = 0) + \mathbb{Z}_2(k_i = 0.5) \pmod{2} \quad (5)$$

$$\nu_i = \mathbb{Z}_2(k_i = 0.5) \quad (6)$$

where k_i is in reduced coordinates. A system is referred to as a strong topological electronic state if $\nu = 1$.

III. RESULTS AND DISCUSSION

The 1T-RhSeTe sample obtained in the experiment was prepared by doping Te with Se, with an exact stoichiometry of $\text{Rh}_{1.01}\text{Se}_{1.05}\text{Te}_{0.94}$. Two potential doping structures, designated as type-I and type-II, are illustrated in Fig. 1(a) and (b) respectively. In the Type-I doping of 1T-RhSeTe, Te atoms are substituted by Se atoms in a linear configuration, resulting in a zigzag arrangement of Te and Se atoms. This arrangement disrupts the inherent triple rotational symmetry of 1T-RhTe₂ and leads to a slightly shorter Se-Rh bond compared to the Te-Rh bond, thereby reducing the symmetry to P2₁/m (No. 11). In contrast, Type-II doping 1T-RhSeTe involves the replacement of Te atoms by

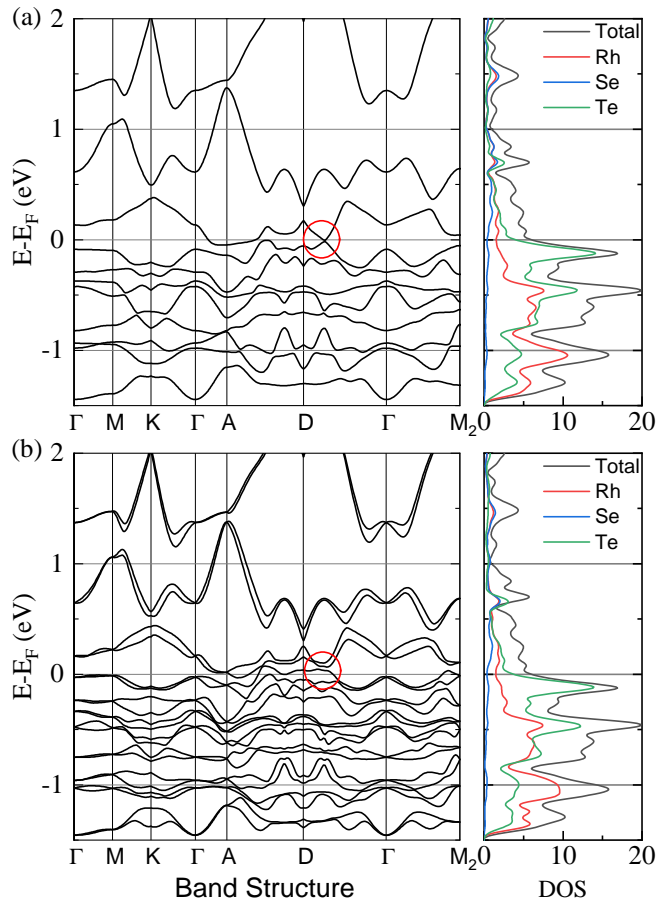


FIG. 3: Band structure and density of states of the 1T-RhSeTe (a) without SOC and (b) including SOC obtained from DFT calculations. There is a Dirac point between D and Γ .

Se atoms within a plane, where Te and Se atoms are distributed in planes, disrupting only the pre-existing -3 symmetry and reducing the symmetry to P3m1 (No. 156). The symmetry of Type-I doped 1T-RhSeTe, which is P2₁/m (No. 11), is lower than that of Type-II doping 1T-RhSeTe [P3m1 (No. 156)]. Both of these symmetries are lower than the P-3m1 (No. 164) symmetry of 1T-RhTe₂.

The lattice constants of the two structures following structural relaxation are presented in Tab I. Type-II doping of 1T-RhSeTe occupies a larger portion of the lattice within the plane, and the two different lengths of Se-Rh and Te-Rh bonds are forced to twist onto the same plane, resulting in a higher energy state compared to Type-I of doping 1T-RhSeTe. Significantly, the lattice constants of Type-I doping 1T-RhSeTe are more closely aligned with experimental measurements, suggesting that the experimental measured 1T-RhSeTe is more likely to conform to Type-I doping. Consequently, we only consider the Type-I doping structure of 1T-RhSeTe in the subsequent analysis.

Phonon dispersion represents a fundamental approach

to assessing the the dynamic stability of a system. The calculated phonon dispersions of 1*T*-RhSeTe are presented in Fig. 2. The absence of imaginary phonon modes in 1*T*-RhSeTe is indicative of its dynamic stability. The phonon dispersion can be classified into two distinct regions based on the vibration frequency. In the high-frequency region ($\omega \geq 110 \text{ cm}^{-1}$), the majority of the phonons are composed of the vibration modes of Se and Te atoms. The Se atoms, which have the lowest mass, contribute the most to the higher-frequency phonons. The Te atoms engage in a seesaw-like resonance around the neighboring Rh atoms with Se atoms, thereby contributing to an additional portion of high-frequency phonons. In the low-frequency region, the phonons are formed by a combination of the vibrational modes of Rh and Te atoms, as these atoms are heavier and more localized in frequency space than Se atoms.

The calculated Eliashberg spectral and integrated electron-phonon coupling strength are plotted in the right panel of Fig. 2. The distribution of the Eliashberg spectral function, $\alpha^2 F(\Omega)$, in the high-frequency region is almost the same as in the low-frequency region. Notably, the vibration frequencies of the heavier elements, including Rh, Se, and Te, predominantly fall within the low-frequency range of 0-200 cm^{-1} . This behavior mirrors findings from electron-phonon coupling calculations in heavier element superconductors, such as LaBi₃ and LaCuSb₂, where electron-phonon interactions are concentrated in the lower vibration frequency range[41, 42].

The electron-phonon coupling in the low-frequency region peaks at around $\omega \sim 25 \text{ cm}^{-1}$, with obvious in-plane vibration modes around the M-K line. As indicated by Eq. (1), these in-plane vibration modes can result in a more pronounced electron-phonon coupling effect, thereby enhancing superconductivity. Around $\omega \sim 180 \text{ cm}^{-1}$ in the high-frequency region, there is another electron-phonon coupling peak, which is mainly dominated by the seesaw-like vibration modes of Se and Te atoms.

Utilizing MLWFs, we derive the isotropic Eliashberg spectral function $\alpha^2 F(\omega)$ for 1*T*-RhSeTe. The integration of $\alpha^2 F(\omega)$ yields the total EPC constant $\lambda = 2.02$ and the logarithmic average frequency $\omega_{\log} = 3.15 \text{ meV}$, indicating a strong electron-phonon coupling in the material. T_c is estimated using the modified McMillan equation by Allen and Dynes. We select $\mu^* = 0.16 \text{ eV}$ considering the heavy elements Rh, Se, and Te. Consequently, we obtain $T_c = 4.61 \text{ K}$, which is remarkably close to the experimental value of 4.72 K [26]. This calculation lends credence to the system's classification as a BCS superconductor, bolstering the validity of our methods.

The energy band structure of 1*T*-RhSeTe is determined using QE, with and without SOC, as illustrated in Fig. 3. In the absence of SOC, the four energy bands closest to the Fermi level are distinctly separated from the remaining bands, exhibiting clear differentiation. It is noteworthy that the two energy bands in closest proximity to the Fermi level exhibit a band crossing along the

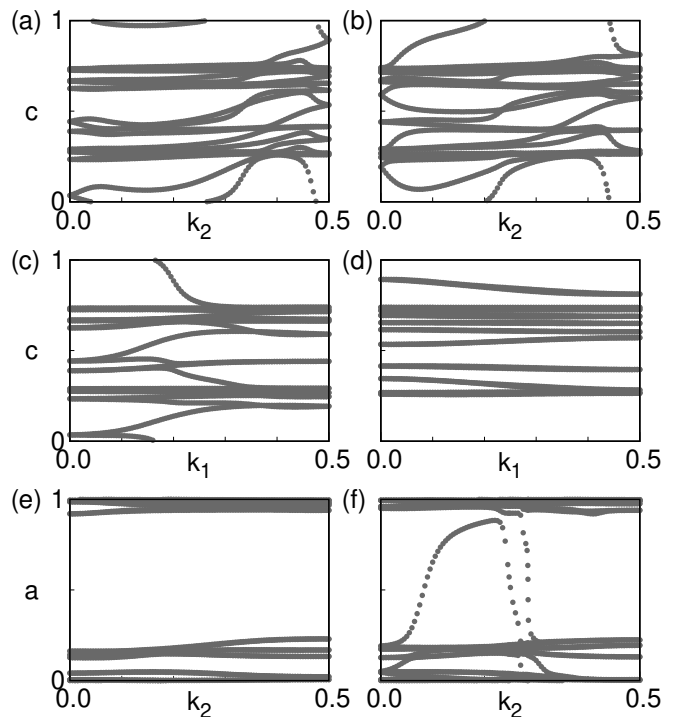


FIG. 4: The evolution of WCCs in the six planes of in Brillouin Zone. The \mathbb{Z}_2 invariants are (a) $k_1 = 0.0$, $k_2 - k_3$ plane: $\mathbb{Z}_2 = 1$ (b) $k_1 = 0.5$, $k_2 - k_3$ plane: $\mathbb{Z}_2 = 0$ (c) $k_2 = 0.0$, $k_1 - k_3$ plane: $\mathbb{Z}_2 = 1$ (d) $k_2 = 0.5$, $k_1 - k_3$ plane: $\mathbb{Z}_2 = 0$ (e) $k_3 = 0.0$, $k_1 - k_2$ plane: $\mathbb{Z}_2 = 0$ (f) $k_3 = 0.5$, $k_1 - k_2$ plane: $\mathbb{Z}_2 = 1$.

D- Γ direction. This crossing point is located very close to the Fermi level (-0.01 eV) and exhibits a linear dispersion, resulting in the formation of Dirac fermions that are analogous to the Dirac points observed in graphene. The Fermi velocity at this point is $v_f = 1.71 \times 10^5 \text{ ms}^{-1}$, which is much lower than that of graphene ($\sim 10^6 \text{ ms}^{-1}$). This reduction in Fermi velocity can be attributed to the fact that these two bands are primarily derived from the p orbitals of Te. Given that the atomic mass of Te is significantly greater than that of C, the effective Fermi velocity is consequently much smaller than that observed in graphene.

A peak in the density of states (DOS) is observed approximately 0.1 eV below the Fermi level, predominantly contributed by the Te atoms. This van Hove singularity in the electron band, associated with the Te atoms, is beneficial for the formation of superconductivity. Additionally, it is noteworthy that this van Hove singularity originates from a flat band along the Γ -M direction. In conjunction with the aforementioned analysis of the low-frequency phonons contributed by Te atoms, it is proposed that this in-plane Γ -M flat band is pivotal for the emergence of superconductivity. Building upon the findings of previous on cuprate superconductors, we propose that electron doping or applying pressure could significantly enhance the superconductivity of 1*T*-RhSeTe, po-

tentially approaching the McMillan limit.

In consideration of the SOC effect, the calculated band structure and DOS for 1T-RhSeTe are presented in Fig. 3(b). In comparison to the band structures without the SOC effect, the band structures undergo significant changes due to the pronounced SOC resulting from the large atomic mass. Each energy band splits into two bands when including SOC, demonstrating that the 1T-RhSeTe system adheres to time-reversal symmetry. The energy and momentum positions of the Dirac cone in the Γ -D line are roughly 151 meV (another suspected Dirac cone at 115 MeV) above the Fermi energy level. The results of the calculation indicated the presence of topological non-trivial states in 1T-RhSeTe.

FIG.4 illustrates the evolution of WCCs in the six planes of the Brillouin Zone. Three planes exhibit a topologically nontrivial state, leading to the determination of the topological \mathbb{Z}_2 index for 1T-RhSeTe represented as (1 ; 0 0 1). The first \mathbb{Z}_2 index is the strong index, while the last three \mathbb{Z}_2 numbers are the weak indices. This topological \mathbb{Z}_2 index indicates that 1T-RhSeTe has a strongly topological electronic state.

IV. CONCLUSIONS

In conclusion, theoretical calculations have been conducted on 1T-RhSeTe, which has been identified as a type of superconductor exhibiting topological electronic states. A doping structure and atomic arrangement for

1T-RhSeTe are constructed that optimizes the material's properties. The integrity of the constructed doping structure is validated through phonon calculations. The analysis of the electron-phonon coupling using the EPW method has confirmed the existence of a robust electron-phonon interaction in 1T-RhSeTe. This has led to the determination of total EPC constant $\lambda = 2.02$, the logarithmic average frequency $\omega_{\log} = 3.15$ meV and $T_c = 4.61$ K, consistent with experimental measurements and indicative of its classification as a BCS superconductor. The band structure analysis revealed the presence of Dirac-like band crossing points, van Hove singularities, and a flat band. The confirmation of the topological non-trivial electronic structures of 1T-RhSeTe is achieved through the evolution of WCCs. The coexistence of superconductivity and topological electronic states in 1T-RhSeTe indicates that it may be a promising candidate for topological superconductivity.

V. ACKNOWLEDGMENTS

This work is supported by the National Natural Science Foundation of China (Grant No. 12204400), Science Research Project of Hebei Education Department (Grant No. QN2022169), Natural Science Foundation of Hebei Province (Grant No. A2022203010), Innovation Capability Improvement Project of Hebei province (Grant No. 22567605H). T. Z. and R. F. contributed equally to this work.

-
- [1] D. Di Sante, P. K. Das, C. Bigi, Z. Ergönenc, N. Gürtler, J. A. Krieger, T. Schmitt, M. N. Ali, G. Rossi, R. Thomale, C. Franchini, S. Picozzi, J. Fujii, V. N. Strocov, G. Sangiovanni, I. Vobornik, R. J. Cava, and G. Panaccione, Three-Dimensional Electronic Structure of the Type-II Weyl Semimetal WTe_2 , *Physical Review Letters* **119**, 026403 (2017).
- [2] F. Wu, T. Lovorn, E. Tutuc, I. Martin, and A. H. MacDonald, Topological Insulators in Twisted Transition Metal Dichalcogenide Homobilayers, *Physical Review Letters* **122**, 086402 (2019).
- [3] S. Wu, V. Fatemi, Q. D. Gibson, K. Watanabe, T. Taniguchi, R. J. Cava, and P. Jarillo-Herrero, Observation of the quantum spin Hall effect up to 100 kelvin in a monolayer crystal, *Science* **359**, 76 (2018).
- [4] D. Costanzo, S. Jo, H. Berger, and A. F. Morpurgo, Gate-induced superconductivity in atomically thin MoS2 crystals, *Nature Nanotechnology* **11**, 339 (2016).
- [5] Y. Fang, J. Pan, J. He, R. Luo, D. Wang, X. Che, K. Bu, W. Zhao, P. Liu, G. Mu, H. Zhang, T. Lin, and F. Huang, Structure re-determination and superconductivity observation of bulk 1t mos2, *Angewandte Chemie International Edition* **57**, 1232 (2018).
- [6] E. Bruyer, D. Di Sante, P. Barone, A. Stroppa, M.-H. Whangbo, and S. Picozzi, Possibility of combining ferroelectricity and Rashba-like spin splitting in monolayers of the 1T-type transition-metal dichalcogenides MX_2 (M=Mo,W;X=S,Se,Te), *Physical Review B* **94**, 195402 (2016).
- [7] J. Strachan, A. F. Masters, and T. Maschmeyer, 3R-MoS2 in Review: History, Status, and Outlook, *ACS Applied Energy Materials* **4**, 7405 (2021).
- [8] C.-S. Lian, C. Si, and W. Duan, Anisotropic Full-Gap Superconductivity in 2M-WS2 Topological Metal with Intrinsic Proximity Effect, *Nano Letters* **21**, 709 (2020).
- [9] W.-Y. He, B. T. Zhou, J. J. He, N. F. Q. Yuan, T. Zhang, and K. T. Law, Magnetic field driven nodal topological superconductivity in monolayer transition metal dichalcogenides, *Communications Physics* **1**, 1 (2018).
- [10] C.-X. Zhao, J.-N. Liu, B.-Q. Li, D. Ren, X. Chen, J. Yu, and Q. Zhang, Multiscale Construction of Bifunctional Electrocatalysts for Long-Lifespan Rechargeable Zinc-Air Batteries, *Advanced Functional Materials* **30**, 2003619 (2020).
- [11] A. F. Kusmartseva, B. Sipoš, H. Berger, L. Forro, and E. Tutis, Pressure Induced Superconductivity in Pristine 1T- $TiSe_2$, *Physical Review Letters* **103**, 236401 (2009).
- [12] R. C. Xiao, P. L. Gong, Q. S. Wu, W. J. Lu, M. J. Wei, J. Y. Li, H. Y. Lv, X. Luo, P. Tong, X. B. Zhu, and Y. P. Sun, Manipulation of type-I and type-II Dirac points in $PdTe_2$ superconductor by external pressure, *Physical Review B* **96**, 075101 (2017).

- [13] Q. L. He, H. Liu, M. He, Y. H. Lai, H. He, G. Wang, K. T. Law, R. Lortz, J. Wang, and I. K. Sou, Two-dimensional superconductivity at the interface of a Bi₂Te₃/FeTe heterostructure, *Nature Communications* **5**, 4247 (2014).
- [14] G. Ermolaev, K. Voronin, D. G. Baranov, V. Kravets, G. Tselikov, Y. Stebunov, D. Yakubovsky, S. Novikov, A. Vyshnevyy, A. Mazitov, I. Kruglov, S. Zhukov, R. Romanov, A. M. Markeev, A. Arsenin, K. S. Novoselov, A. N. Grigorenko, and V. Volkov, Topological phase singularities in atomically thin high-refractive-index materials, *Nature Communications* **13**, 2049 (2022).
- [15] M. Yan, H. Huang, K. Zhang, E. Wang, W. Yao, K. Deng, G. Wan, H. Zhang, M. Arita, H. Yang, Z. Sun, H. Yao, Y. Wu, S. Fan, W. Duan, and S. Zhou, Lorentz-violating type-II Dirac fermions in transition metal dichalcogenide PtTe₂, *Nature Communications* **8**, 10.1038/s41467-017-00280-6 (2017).
- [16] T. T. Tanisha, M. S. Hossain, N. T. Hiramony, A. Rasul, M. Z. Hasan, and Q. D. M. Khosru, *Tunable Topological Phase Transitions in a Piezoelectric Janus Monolayer*, Tech. Rep. (arXiv:2401.13124, 2024).
- [17] M. Sato and Y. Ando, Topological superconductors: a review, *Reports on Progress in Physics* **80**, 076501 (2017).
- [18] K.-Y. Gu, T.-C. Luo, J. Ge, and J. Wang, Superconductivity in topological materials, *Acta Physica Sinica* **69**, 020301 (2020).
- [19] S.-B. Zhang, W. B. Rui, A. Calzona, S.-J. Choi, A. P. Schnyder, and B. Trauzettel, Topological and holonomic quantum computation based on second-order topological superconductors, *Physical Review Research* **2**, 043025 (2020).
- [20] A. Y. Kitaev, Fault-tolerant quantum computation by anyons, *Annals of Physics* **303**, 2 (2003).
- [21] V. Lahtinen and J. Pachos, A Short Introduction to Topological Quantum Computation, *SciPost Physics* **3**, 021 (2017).
- [22] C. Nayak, S. H. Simon, A. Stern, M. Freedman, and S. Das Sarma, Non-Abelian anyons and topological quantum computation, *Reviews of Modern Physics* **80**, 1083 (2008).
- [23] S. D. Sarma, M. Freedman, and C. Nayak, Majorana zero modes and topological quantum computation, *npj Quantum Information* **1**, 1 (2015).
- [24] L. Fidkowski, Entanglement Spectrum of Topological Insulators and Superconductors, *Physical Review Letters* **104**, 130502 (2010).
- [25] X.-L. Qi and S.-C. Zhang, Topological insulators and superconductors, *Reviews of Modern Physics* **83**, 1057 (2011).
- [26] C. Patra, T. Agarwal, Arushi, P. Manna, N. Bhatt, R. S. Singh, and R. P. Singh, *Superconducting Properties of Topological Semimetal 1T-RhSeTe*, Tech. Rep. (arXiv:2311.01019, 2023).
- [27] S. Geller, The Crystal Structures of RhTe and RhTe₂, *Journal of the American Chemical Society* **77**, 2641 (1955).
- [28] F. E. Lurgo, F. Pomiro, R. E. Carbonio, and R. D. Sanchez, Synthesis and structural, magnetic, electric, and thermoelectric characterization of layered Rh_{1-x}Ir_xTe₂ (0 ≤ x ≤ 1), *Physical Review B* **105**, 104104 (2022).
- [29] G. Kresse and J. Hafner, Ab initio molecular dynamics for liquid metals, *Physical Review B, Condensed Matter* **47**, 558 (1993).
- [30] J. P. Perdew, K. Burke, and M. Ernzerhof, Generalized Gradient Approximation Made Simple, *Physical Review Letters* **77**, 3865 (1996).
- [31] G. Kresse and D. Joubert, From ultrasoft pseudopotentials to the projector augmented-wave method, *Physical Review B* **59**, 1758 (1999).
- [32] J. Klimeš, D. R. Bowler, and A. Michaelides, Chemical accuracy for the van der waals density functional, *Journal of Physics: Condensed Matter* **22**, 022201 (2009).
- [33] P. Giannozzi, O. Andreussi, T. Brumme, O. Bunau, M. B. Nardelli, M. Calandra, R. Car, C. Cavazzoni, D. Ceresoli, M. Cococcioni, N. Colonna, I. Carnimeo, A. D. Corso, S. d. Gironcoli, P. Delugas, R. A. DiStasio, A. Ferretti, A. Floris, G. Fratesi, G. Fugallo, R. Gebauer, U. Gerstmann, F. Giustino, T. Gorni, J. Jia, M. Kawamura, H.-Y. Ko, A. Kokalj, E. Küçükbenli, M. Lazzeri, M. Marsili, N. Marzari, F. Mauri, N. L. Nguyen, H.-V. Nguyen, A. Otero-de-la Roza, L. Paulatto, S. Poncé, D. Rocca, R. Sabatini, B. Santra, M. Schlipf, A. P. Seitsonen, A. Smogunov, I. Timrov, T. Thonhauser, P. Umari, N. Vast, X. Wu, and S. Baroni, Advanced capabilities for materials modelling with Quantum ESPRESSO, *Journal of Physics: Condensed Matter* **29**, 465901 (2017).
- [34] A. A. Mostofi, J. R. Yates, G. Pizzi, Y.-S. Lee, I. Souza, D. Vanderbilt, and N. Marzari, An updated version of wannier90: A tool for obtaining maximally-localised wannier functions, *Computer Physics Communications* **185**, 2309 (2014).
- [35] A. A. Mostofi, J. R. Yates, Y.-S. Lee, I. Souza, D. Vanderbilt, and N. Marzari, wannier90: A tool for obtaining maximally-localised Wannier functions, *Computer Physics Communications* **178**, 685 (2008).
- [36] P. B. Allen, Neutron Spectroscopy of Superconductors, *Physical Review B* **6**, 2577 (1972).
- [37] P. B. Allen and R. C. Dynes, Transition temperature of strong-coupled superconductors reanalyzed, *Physical Review B* **12**, 905 (1975).
- [38] Q. Wu, S. Zhang, H.-F. Song, M. Troyer, and A. A. Soluyanov, Wanniertools: An open-source software package for novel topological materials, *Computer Physics Communications* **224**, 405 (2018).
- [39] R. Yu, X. L. Qi, A. Bernevig, Z. Fang, and X. Dai, Equivalent expression of Z₂ topological invariant for band insulators using the non-Abelian Berry connection, *Physical Review B* **84**, 075119 (2011).
- [40] C. L. Kane and E. J. Mele, Z₂ Topological Order and the Quantum Spin Hall Effect, *Physical Review Letters* **95**, 146802 (2005).
- [41] W. Chen, T. Shen, Y. Feng, C. Liu, X. Liu, and Y. Wu, Sensitive biosensing based on a d-type photonic crystal fiber, *Physica Scripta* **98**, 105531 (2023).
- [42] K. Akiba and T. C. Kobayashi, Phonon-mediated superconductivity in the sb square-net compound lacusb₂, *Physical Review B* **107**, 245117 (2023).
- [43] S. Poncé, E. R. Margine, C. Verdi, and F. Giustino, EPW: Electron-phonon coupling, transport and superconducting properties using maximally localized Wannier functions, *Computer Physics Communications* **209**, 116 (2016).
- [44] A. A. Soluyanov and D. Vanderbilt, Wannier representation of Z₂ topological insulators, *Physical Review B* **83**, 035108 (2011), arXiv:1009.1415 [cond-mat].